Katja Burek | Dr. Joachim Dengler | Dr. Franziska Emmerling |
Ines Feldmann | Prof. Michael U. Kumke | Dr. Julia Stroh

Lanthanide Luminescence Revealing the Phase Composition in Hydrating Cementitious Systems

Suggested citation referring to the original publication:
ChemistryOpen 8 (2019) 12
DOI https://doi.org/10.1002/open.201900249
ISSN (online) 2191-1363

ChemPubSoc Europe

DOI: 10.1002/open.201900249

Open Access ChemistryOPEN Full Papers

Lanthanide Luminescence Revealing the Phase Composition in Hydrating Cementitious Systems

Katja Burek[+],*[a] Joachim Dengler,[c] Franziska Emmerling,*[b] Ines Feldmann,[b] Michael U. Kumke,*[a] and Julia Stroh[+]*[b]

The hydration process of Portland cement in a cementitious system is crucial for development of the high-quality cement-based construction material. Complementary experiments of X-ray diffraction analysis (XRD), scanning electron microscopy (SEM) and time-resolved laser fluorescence spectroscopy (TRLFS) using europium (Eu(III)) as an optical probe are used to analyse the hydration process of two cement systems in the absence and presence of different organic admixtures. We show that different analysed admixtures and the used sulphate carriers in each cement system have a significant influence on the hydration process, namely on the time-dependence in the formation of different hydrate phases of cement. Moreover, the effect of a particular admixture is related to the type of sulphate carrier used. The quantitative information on the amounts of the crystalline cement paste components is accessible via XRD analysis. Distinctly different morphologies of ettringite and calcium–silicate–hydrates (C–S–H) determined by SEM allow visual conclusions about formation of these phases at particular ageing times. The TRLFS data provides information about the admixture influence on the course of the silicate reaction. The dip in the dependence of the luminescence decay times on the hydration time indicates the change in the structure of C–S–H in the early hydration period. Complementary information from XRD, SEM and TRLFS provides detailed information on distinct periods of the cement hydration process.

1. Introduction

Chemical admixtures based on organic acids and polycarboxylate ether (PCE) retard the hydration process of Portland cement, thus influencing the properties of the hardened material. The determination of the involved reactions is challenging due to the complex phase composition of the hydrated cementitious matrix. A deeper mechanistic understanding of the admixture influence during the hydration process is needed to avoid undesirable consequences of their application. Further, tailoring the admixture chemistry enables controlling both the properties of the fresh cement paste and the development of the hardened cement matrix.

The non-hydrated Portland cement consists of four main phases: tricalcium silicate (Ca_3SiO_5, C_3S), dicalcium silicate (Ca_2SiO_4, C_2S), tricalcium aluminate ($Ca_3Al_2O_6$, C_3A) and dicalcium aluminate–ferrite ($Ca_2(Al_x,Fe_{(1-x)})_2O_5$, $C_2(A,F)$).[1] Thus, two main types of reactions occur during the cement hydration: the hydration of calcium silicate phases (silicate reaction) and the hydration of calcium aluminate phases (aluminate reaction). During the latter, aluminate phases C_3A and $C_2(A,F)$ react with sulphate ions released form the dissolution of the sulphate carrier ($CaSO_4$, its hemi- $CaSO_4 \cdot 0.5H_2O$ or dihydrate $CaSO_4 \cdot 2H_2O$) (Eq. 1). The product of these reactions within first 24 h is the aluminate–ferrite tri (AFt)[1] hydrate phase ettringite $[Ca_3Al(OH)_6]_2 \cdot (SO_4)_3 \cdot 26H_2O$ (Eq. 2). During further ageing, ettringite can transform into the aluminate–ferrite mono (AFm)[2] hydrate phases. This process can be understood as redistribution of available sulfate ions to dissolved aluminates in the cementitious system.

$$Ca_3Al_2O_6 + 3CaSO_4 \cdot 2H_2O + 26H_2O \rightarrow [Ca_3Al(OH)_6]_2 \cdot (SO_4)_3 \cdot 26H_2O \quad (1)$$

$$Ca_2(Al_x,Fe_{(1-x)})_2O_5 + 3CaSO_4 \cdot 2H_2O + Ca(OH)_2 + 25H_2O \rightarrow [Ca_3Al(OH)_6]_2 \cdot (SO_4)_3 \cdot 26H_2O \quad (2)$$

[a] K. Burek,[+] Prof. M. U. Kumke
Institute for Chemistry, University Potsdam, Karl-Liebknecht-Straße 24–25, Potsdam-Golm (Germany)
E-mail: burek@uni-potsdam.de
kumke@uni-potsdam.de

[b] Dr. F. Emmerling, I. Feldmann, Dr. J. Stroh[+]
BAM Federal Institute for Materials Research and Testing, Richard-Willstätter-Str. 11, 12489 Berlin-Adlershof (Germany)
E-mail: julia.stroh@bam.de
franziska.emmerling@bam.de

[c] Dr. J. Dengler
BASF Construction Solutions GmbH, E-EDE/BT AT, B08, Dr-Albert-Frank-Straße 32, 83308 Trostberg (Germany)

[+] These authors contributed equally to this work

Supporting information for this article is available on the WWW under https://doi.org/10.1002/open.201900249

[1] The general formula of the AFt phases is $[Ca_3(Al,Fe)(OH)_6 \cdot 12H_2O]_2 \cdot X_3 \cdot nH_2O$, where X can be one bivalent or two monovalent anions (e.g. sulfate, carbonate, chloride, hydroxide)

[2] The general formula of the AFm phases is $[Ca_2(Al,Fe)(OH)_6]_2 \cdot X \cdot nH_2O$, where X can be one bivalent or two monovalent anions (e.g. sulfate, carbonate, chloride, hydroxide) or their combinations (e.g. monocarbohydroxyaluminate $[Ca_2Al(OH)_6]_2 \cdot (CO_3)_{0.5} \cdot (OH) \cdot 5.5H_2O$

The silicate reactions produce calcium silicate hydrate (C–S–H) phases, which can have the variable stoichiometry and cause the main binding capacity of hardened cement paste (Eq. 2).

$$nCa_3SiO_5 + (p + 3n - m)H_2O \rightarrow mCaO \cdot nSiO_2 \cdot pH_2O + (3n - m)Ca(OH)_2 \quad (3)$$

$$nCa_2SiO_4 + (p + 2n - m)H_2O \rightarrow mCaO \cdot nSiO_2 \cdot pH_2O + (2n - m)Ca(OH)_2 \quad (4)$$

Carboxylic acids are used as retarding admixtures and can be found in the compositions of flow modifiers.[2] Citric and tartaric acids are known to retard the hydration of silicates by slowing down the dissolution of C_3S.[3,4] Citric acid reduces further the early strength of the hardened cement paste.[5] There are evidences for the influence of citric acid on the hydration of aluminate and formation of ettringite.[6] The origin of these influences is discussed contradictorily.[3,6] G. Möschner *et al.* explained the retarded dissolution of the clinker grains by the sorption of citrate to the clinker surface and the formation of a protective layer around the clinker grains.[3] Tartaric acid was found to delay the ettringite formation by poisoning the nuclei growth or by formation of a calcium tartrate layer on C_3A.[4,7] The influence of PCEs, which are used as effective superplasticizers, is described as retardation of the stiffening. The reason for this seems to be the preferential adsorption of these comb-like polymers on the unhydrated aluminate phases, which are the crystallization places for the ettringite formation.[2,8,9] Evidences of the changes in the aluminate reactions are available analysing their products, which are crystalline hydrate phases (AFt, AFm, portlandite ($Ca(OH)_2$)). For this, X-ray diffraction analysis (XRD) was used to obtain information on crystalline substances. On the other hand, C–S–H are poorly crystalline making XRD of limited use. Here, complementary analytical techniques are needed to characterize the influence of admixtures. Recently, europium-doped C–S–H phases were investigated using Eu(III) luminescence to probe structural properties.[10] Using time-resolved laser fluorescence spectroscopy (TRLFS), structural information on the C–S–H phases can be obtained regardless of their crystallinity. The identification of the Eu(III) location within the cement matrix is improved by comparison with respective luminescence data of the pure (reference) hydrate phases.

Here, we present results obtained in the investigation of the admixture influence in the early stage (first 24 h) of the Portland cement hydration as well as after 28 d. For the first time, we applied XRD and TRLFS as complementary techniques to investigate the formation of the different phases (and their time evolution) during the early cement hydration and the effects of different organic admixtures on it. The achieved results were supported by the scanning electron microscopy (SEM). SEM images allowed morphological phase analysis based on the distinct morphological differences between hydrate phases. Each of the analytical techniques has its marked advantages to evaluate certain parts of the hydration process. By combining the complementary techniques, we could show that an improved, more detailed, description can be achieved, in which differences in the formation of C–S–H and ettringite were resolved depending on the presence and the type of admixture used.

Experimental Section

Sample Preparation

A mixture of 90 $\%_{wt.}$ Portland cement (CEM I Milka, HeidelbergCement AG, Germany) and 10 $\%_{wt.}$ calcium aluminate cement (Fondu ciment, Kerneos, France) was prepared. Afterwards, 4 $\%_{wt.}$ of i) calcium sulfate hemihydrate $CaSO_4 \cdot 0.5H_2O$ (Schwarze Pumpe, Germany) (CSI) or ii) of calcium sulfate $CaSO_4$ (BASF, Germany) (CSII) was added to this basic cementitious system (CS). Finally, 3 $\%_{wt.}$ of rutile TiO_2 was added to each cement system as internal standard. The resulting absolute component amounts for both cementitious systems are given in Table 1. Series of cement paste samples were prepared from each CS with water-to-cement ratio (w/c) of 0.5. In each sample series, organic admixtures based on carboxylic acids (citric acid, tartaric acid) as well as the complex hydration control agent (HCA)[11] were added with mixing water. The HCA was dry mixed from 2-hydroxy-2-sulfonato acetic acid, ethylene carbonate and polycarboxylate in the ratio of 1:1:0.25, respectively. The polycarboxylate was a copolymer from acrylic acid and 2-acrylamido-2-methylpropansulfonic acid. The concentrations of the admixture solutions were chosen specifically for each CS and are given in Table 1. Additionally, reference samples were prepared without any admixture. For luminescence studies, the cement paste samples were doped with aqueous $EuCl_3$ solutions. The concentration of $EuCl_3$ was chosen to achieve an Eu(III) amount of 10 µmol/g CS. The water containing in the $EuCl_3$ solutions was considered by calculation of w/c. After different hydration times (1, 2, 4, 6, 10, 16, 24 h, and 28 d), the samples were gently dried in a vacuum dryer at room temperature to remove the excess water and thus to stop the hydration process. We avoided applications of further drying methods typically used to stop the cement hydration (e.g. solvent drying, freeze drying), since all of them change the phase composition of hydrated cement paste, although to a different extent.[12] Dried cement samples were ground by hand in the agate mortar and used for analyses. In the meantime, the sample material was stored in tightly closed glass vials.

Powder X-Ray Diffraction Analysis (XRD)

XRD was carried out to achieve information on the composition of crystalline phase in the cement paste samples. The powder samples

Table 1. Percentage of cementitious components and applied admixtures.

Component	CSI amount [$\%_{wt.}$]	CSII amount [$\%_{wt.}$]
Portland cement (CEM I)	84.02	84.02
Calcium aluminate cement	9.34	9.34
Calcium sulfate hemihydrate	3.73	–
Calcium sulfate	–	3.73
Titanium dioxide	2.91	2.91
Admixture	c [$\%_{bwoc}$[iv]]	c [$\%_{bwoc}$]
Citric acid	0.25	0.15
L-(+)-tartaric acid	0.15	0.10
HCA	0.30	0.25

[iv] bwoc – by weight of cement

were filled into the plate sample holders. The measurements were carried out on a Bragg-Brentano diffractometer (D8 Advance, Bruker AXS, Germany) with a copper X-ray source ($Cu_{K\alpha}$) and a LYNXEYE XE-T detector. The tube was operated at 40 keV and 40 mA. The diffractograms were acquired in the 2θ range of 5–60° with the step size of 0.016° and 1 s per step exposure time.

The qualitative phase analysis was carried out using DIFFRAC.EVA software (Bruker AXS, Germany) with implemented PDF-2 2016 database. Based on the results of the phase identification, Rietveld refinements were performed using the Topas software (Bruker AXS, Germany) to determine the quantitative phase composition of the crystalline components of the hydrated cement samples. The determined percentages of crystalline phases are related to the total crystalline part of the cement paste, thus excluding the nanocrystalline/amorphous part. The structural data for the Rietveld refinement analyses was taken from the Inorganic Crystal Structure Database (ICSD, FIZ Karlsruhe Leibnitz Institute for Information Infrastructure, Germany). First, the Rietveld analyses of unhydrated CSI and CSII were carried out by including the lattice parameters, Lorentzian crystallite size, and the atomic positions of unhydrated cement phases in the refinement. The results of the phases analyses on the CSI and CSII are summarized in the Table SI1. For the quantification of the hydrated samples, the refined structural parameters of the unhydrated phases were adopted and fixed during the refinement. Following parameters were refined: background, zero error, scale factor, and Lorentzian crystal size. Additionally, lattice parameters and atomic positions of the hydrate phases were refined.

Scanning Electron Microscopy (SEM)

SEM imaging was carried out at a scanning electron microscope (FEI XL30, Philips, USA) using secondary electron detector. The images were captured at the acceleration voltage of 20 kV and the working distance of 6.5 mm. The powders prepared from the dried cement paste were sputtered with gold to improve the surface conductivity. Ettringite and C–S–H phases could be identified on their characteristic morphology, which is well documented being hexagonal prismatic needles for ettringite and fibrous for C–S–H phases.[13–16]

Luminescence Spectroscopy

Time-resolved laser fluorescence spectroscopy (TRLFS) was used to analyse the luminescence of Eu(III) in 1 g of each cement sample. A pulsed Nd:YAG laser (QuantaRay, Spectra Physics, USA) with a repetition rate of 20 Hz was coupled to an optical parametric oscillator (OPO, GWU Lasertechnik, Germany), serving as light source for the Eu(III) excitation at $\lambda_{ex} = 394$ nm ($^5L_6 \leftarrow {}^7F_0$ transition). Water and the organic compounds have no absorption band at the used wavelength. An influence of photochemical reactions of the organic compounds due to the temperature or laser power were ruled out by observing a stable luminescence signal over time. An iCCD camera (Andor Technology, iStar iCCD-3202, DH-720-18H-13, United Kingdom) was connected to a spectrograph (Oriel Instrument, MS257, USA) equipped with a 1200 lines/nm and 500 nm blazed grating. The Eu(III) luminescence emission was detected in the spectral range of 575 nm $< \lambda_{em} <$ 635 nm. The time-resolved luminescence kinetics were measured by using the boxcar technique with an initial delay time of $t_l = 10$ µs. A total of 100 accumulations were recorded for each emission spectra. For a full luminescence kinetics, 150 emission spectra collected with increasing the delay times in linear variable steps were acquired (exposure time $t_{exposure} = 1.7$ ms). The gate pulse widths were chosen specifically for each sample and are shown in Table SI2.

The luminescence decay times of Eu(III) were calculated from the decrease of the time-dependent integrals of the $^5D_0 \rightarrow {}^7F_1$ and $^5D_0 \rightarrow {}^7F_2$ emission band by using a multi-exponential function (Eq. 5). In the data fitting procedure, the decay constants of both emission bands were shared.

$$y(t_l) = y_0 + \sum_{n=1}^{N} \left(A_i \exp\left(-\frac{t_l}{\tau_i} \right) \right) \quad (5)$$

Here, $y(t_l)$ is the (integral) luminescence intensity of Eu(III) $^5D_0 \rightarrow {}^7F_1$ or $^5D_0 \rightarrow {}^7F_2$ emission band and t_l the corresponding delay time after the laser flash. The background signal is given by y_0 and the amplitude of the luminescence decay of the i^{th} component by A_i. Eq. 6 can be used to determine the fraction f_j of the luminescence decay with the amplitude A_j for component j.

$$f_j = \frac{A_j \cdot \tau_j}{\sum_{n=1}^{N} (A_i \cdot \tau_i)} \quad (6)$$

The asymmetric ratio R was determined according to Eq. 7 using the integrated luminescence intensity of the $^5D_0$-$^7F_2$ and $^5D_0$-$^7F_1$ band.

$$R = \frac{I(^5D_0 \rightarrow {}^7F_2)}{I(^5D_0 \rightarrow {}^7F_1)} \quad (7)$$

Furthermore, time-resolved area-normalized emission spectra (TRANES) were calculated from emission spectra measured at 10 µs, 100 µs, 200 µs, 500 µs, 1000 µs, 2000 µs, 3000 µs and 4000 µs delay time (gate widths are shown in Table SI2). Here, up to 2000 accumulations were aquired for one emission spectrum. This high accumulation number was chosen to significantly improve the signal-to-noise ratio. Differences in the spectral intensity distribution of area-normalized emission spectra after different delay times point towards the existence of different Eu(III) species in the sample. Each sorbed Eu(III) species is correlated with a specific spectral signature. This fact was further used for a factor analysis of the $^5D_0$-$^7F_2$ emission bands to analyse the relative amount of the existing Eu(III) species.

In the analysis of the spectra, complementary information on the composition of the cement system was used. In the early state of cement hydration, Eu(III) could be sorbed by portlandite, ettringite (AFt) and C–S–H. Additionally, Eu(III)-carbonates and Eu(III)-hydroxides can be formed due to a reaction with CO_2 from the atmosphere and the high pH value. Moreover, in CSII Eu(III) could be sorbed by $CaSO_4$. Based on this information, a Gaussian fitting for each separate reference system was done first. Afterwards, all obtained Gaussian curves were summed up. The resulting function represented the Eu(III) luminescence spectrum of all species (Eq. 8, for more details see Eq. SI1) and was used for the factor analysis of the measured emission spectra. We further used the specific advantage of a time-gated detection scheme. In the analysis, the emission spectra recorded with a delay time of $t_l = 1000$ µs were used. In that case, Eu(III)-hydroxide species were not observed due to their short luminescence decay times (below 100 µs) and consequently, these Eu(III) species could be excluded ($A_1 = 0$) to slightly simplify the highly complex system. In Eq. SI1 the second term $A_2(\ldots)$ corresponded to Eu(III) in portlandite, the third $A_3(\ldots)$ to Eu(III)-carbonates, the fourth $A_4(\ldots)$ to Eu(III) in C–S–H, the fifth $A_5(\ldots)$ to Eu(III) in ettringite and the sixth $A_6(\ldots)$ to Eu(III) in $CaSO_4$. In the case of CSI, no sorption of Eu(III) on $CaSO_4$ was observed and therefore, A_6 was zero.

$$y = y_0 + \sum_{k=1}^{6}\left(A_{k(ratio)} \cdot \sum_{m=1}^{n}\left(\frac{\frac{A_m}{A_{k(ratio)}}}{w_m \cdot \sqrt{\frac{\pi}{2}}} \cdot e^{-2\left(\frac{x-x_m}{w_m}\right)^2}\right)\right) \quad (8)$$

For each reference, the area ratio $A_{k(ratio)}$ of all Gaussian curves was determined. These ratios were fixed in Eq. 8 in order to identify the relative amount of each reference compound in the measured $^5D_0$-$^7F_2$ emission band of Eu(III) in the analysed cement sample. In Eq. 8, $A_{k(ratio)}$ is a free running area factor and contains information about the amount of the k^{th} reference in the cement sample, y_0 is the offset of the $^5D_0$-$^7F_2$ emission band, x_m – the wavelength of the peak maximum, and A_m – the area of the m^{th} Gaussian function. Furthermore, in Eq. 8 the obtained peak maxima of the Gaussian curves in the m^{th} reference were fixed to the wavelength listed in Table SI3. The peak width w_m of the m^{th} Gaussian function and the peak width at half maximum $FWHM_m$ are connected as described by Eq. 9.

$$w_m = \frac{FWHM_m}{\sqrt{\ln(4)}} \quad (9)$$

Eq. 10 was used to calculate the relative amount of each Eu(III) reference f_k in the $^5D_0$-$^7F_2$ emission band of the cement samples at a delay time of $t_1 = 1000$ µs.

$$f_k = \frac{\frac{\frac{A_k}{A_{k(ratio)}} \cdot A_{k(ref)}}{\Phi_k}}{\sum_{k=1}^{6}\left(\frac{\frac{A_k}{A_{k(ratio)}} \cdot A_{k(ref)}}{\Phi_k}\right)} \cdot 100\,\% \quad (10)$$

Here, A_k is the area of the Gaussian peak in the k^{th} reference in the sample, while $A_{k(ref)}$ is representing the area sum of all Gaussian curves of the k^{th} reference Φ_k is the quantum yield of Eu(III) in the k^{th} reference.

A parallel factor analysis (PARAFAC) algorithm, written in the optimization toolbox of Matlab 2018 (*MathWorks*, USA), was used to extract the emission spectra, decay times and speciation of each Eu(III) species in the CSI and CSII samples.[17] In the hydration time dimension, the luminescence decay time of each component has been constrained to a monoexponential decay.[18] For the calculations, the spectral and speciation dimension was set to non-negative.

2. Results

2.1. XRD

The percentages of the crystalline unhydrated cement phases and their hydrates determined using the Rietveld analysis are plotted over time and shown in Figure 1. The consumption of the unhydrated phases and formation of the hydrates was analysed related to the corresponding hydration reactions. The latter can be divided into:

i) the hydration of the calcium silicate phases leading to the formation of C–S–H and portlandite; the amount of calcium silicates includes both tri- and dicalcium silicate phases (Figure 1, right);

ii) the hydration of the calcium aluminate phases; the amount of calcium aluminate phases includes C_3A and $C_2(A,F)$; the product of these reactions within first 24 h is found to be ettringite (Eq. 2) (Figure 1, right). During further ageing, ettringite transformed partially into monocarbohydroxyaluminate[iii] and monocarbohydroxyaluminate–ferrite[3], which were identified in the samples aged for 28 days.

The amounts of the related phases for the silicate reaction are shown in Figure 1, left, and for the aluminate reaction – in Figure 1, right for each analysed cementitious system. The consumption of sulfate carriers (gypsum in CSI or anhydrous calcium sulfate in CSII) is shown in Figure SI1 in comparison with the amount of ettringite formed.

In the CSI samples aged for 1 h, ettringite is found to have an amount of 12% to 14%. Then, the amounts of ettringite achieved values between 19% and 22% after 24 h of hydration and increased slightly to 22%–25% after 28 days of ageing. It shows, that most of the ettringite was formed in CSI within the first hour after the hydration begins. The lowest ettringite amount was observed regardless of the ageing time in the reference sample without any admixture. CSII samples showed a similar pattern of the ettringite formation: 11%–13% of ettringite were formed within first hour of hydration. In the age of 28 days, the amount of ettringite increased to 20%–24%.

Portlandite is a crystalline product of the silicate reactions. In the CSI-based samples, it was first identified in the reference sample after 4 h ageing. In the samples with admixtures, portlandite was identified: after 2 h ageing – in the sample with HCA, after 6 h of ageing – in the sample with tartaric acid, and as longest after 16 h – in the sample with citric acid. In the age of 28 days, similar amounts of 18%–20% of portlandite were identified in the analysed samples. The consumption of calcium silicates is estimated at the total content of C_3S and C_2S and differs significantly depending on the admixture added. It is pronounced in the samples with citric (33%) and tartaric (32%) acids showing the lowest amounts of remaining calcium silicates in the age of 28 days. For comparison, the reference sample showed 38% of calcium silicates remaining after 28 days. For CSII, portlandite formation was observed solely in the samples with and without admixtures aged for 28 days, with similar amounts being between 9%–11%. The highest amount of portlandite (11%) is formed in the reference sample and corresponds to 43% of calcium silicates remaining in this sample. Interestingly, the noticeable consumption of calcium silicates is observed within first 24 h of hydration, where no portlandite crystallisation is identified. The amounts of portlandite formed after 28 days ageing in the samples with admixture added are lower than in the reference sample without admixture. Furthermore, the presence of admixture led to higher consumption of calcium silicates in these samples than in the reference sample. This observation leads to the question, what calcium silicates are consumed for within first 24 h of hydration and in the samples with admixtures – after 28 days of hydration. Since no other crystalline products of the silicate reactions are identified, another question is, in which form the products of the calcium silicate dissolution persist in the cementitious matrices.

[3] $[Ca_2(Al,Fe)(OH)_6]_2 \cdot (CO_3)_{0.5} \cdot (OH) \cdot 5H_2O$

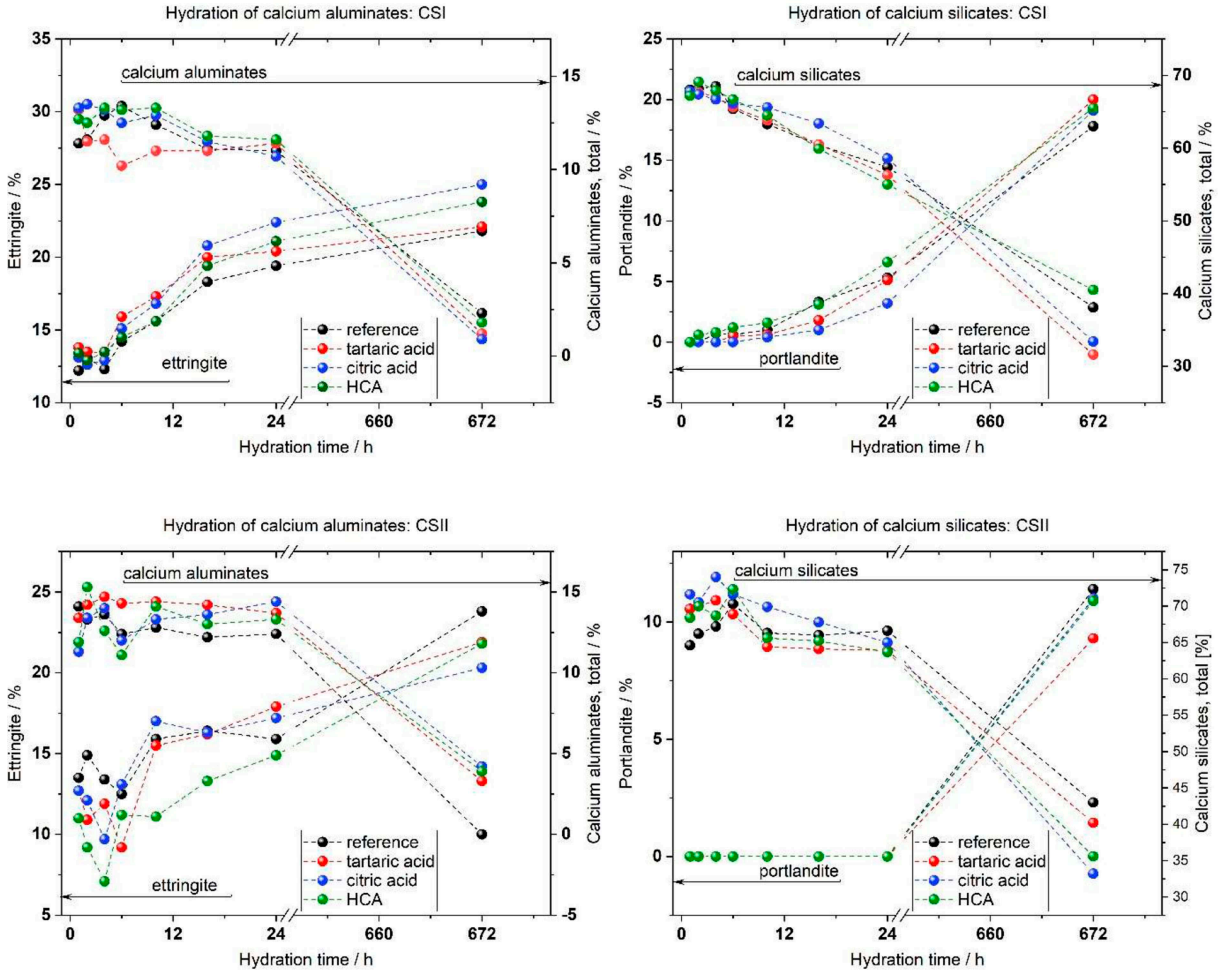

Figure 1. Changes of the phase composition of the samples from CSI (top) and CSII (bottom). Left – the consumption of the calcium aluminates and the formation of ettringite; right – the consumption of the calcium silicates and the formation of portlandite.

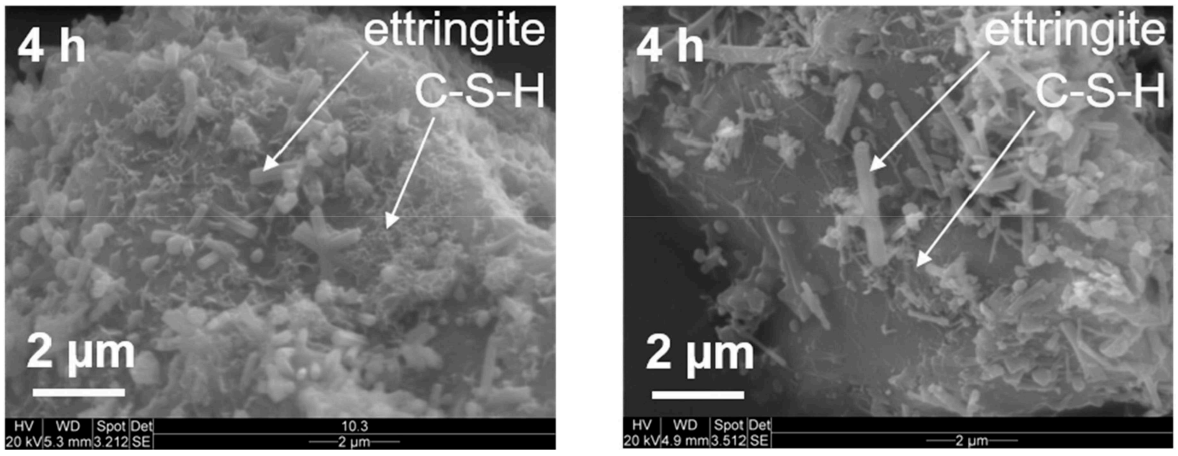

Figure 2. SEM images of the reference samples after 4 h ageing. Left – CSI; right – CSII.

2.2. SEM

The SEM images were taken for the samples aged for 1 h, 4 h, 6 h and 24 h (Figure SI2–3) to analyse the formation of the hydrate phases based on their morphology. The hydrate phases ettringite and C–S–H are identified in the analysed samples and are exemplarily shown in Figure 2. Their presence depends on the ageing time of the samples and on the addition of

admixtures. In general, ettringite is identified after shorter ageing times than C–S–H giving an estimation of the comparable speed of the aluminate versus silicate reaction. The results of the SEM evaluation are discussed below.

Ettringite is formed in both analysed cement systems already in the samples aged for 1 h, thus supporting the results of XRD. The number of crystals, their size and morphology differ depending on the kind of cement system and the presence of admixture. In CSI samples, ettringite crystals are well-shaped hexagonal prisms (Figure SI2). In absence of admixtures, numerous short prismatic crystals are formed already after 1 h covering the surface of the unhydrated cement grains (Figure SI2, a). In the samples based on CSII, the formed ettringite crystals are significantly thinner and longer, appearing as a straw-like cover on the cement grain surfaces (Figure SI3, a). If an admixture was added, the formation of larger ettringite crystals than in the reference samples is observed in both cement systems. In CSI, the lower number of ettringite crystals forms bushes of hexagonal prisms in contrast to crystal cover in the reference samples (Figure SI2, b–d). In the CSII, visually less ettringite crystals are formed either, if compared to the related CSII reference samples (Figure SI3, b–d). Additionally, the crystals in the CSII samples with admixture addition are thicker and clearly hexagonal prismatic in contrast to the reference samples. The decrease of the number of ettringite crystals formed in presence of admixtures can indicate the suppression of the nucleation by admixtures. This effect was observed for tartaric acid by Zhang *et al.*.[4]

The formation of the C–S–H phase is identified on its characteristic tiny fibrous crystals covering the cement grains. In the CSI samples, the C–S–H forms a honeycomb-like cover on the surface of the unhydrated cement grains. In all samples except those with citric acid, the C–S–H phase is found after 4 h ageing. The addition of the citric acid delays its formation: The C–S–H is found in this sample first after 6 h of ageing. In the CSII, the formation of the C–S–H is week and its morphology is not fibrous. This makes the identification of the C–S–H in the CSII samples based on SEM difficult.

2.3. TRLFS – Influence of Hydration Time on Luminescence Decay Times τ_i (i = 1–3)

The luminescence decay kinetics of Eu(III) in CSI and CSII with water, citric acid, tartaric acid as well as HCA in dependence on the hydration time were analysed according to Eq. (5) with N = 3, assuming Eu(III) to be located in at least three distinctly different coordination environments. The obtained luminescence decay times τ_2 and τ_3 showed a relatively sharp decrease of the respective value between 4 h and 6 h hydration time in each case of CSI and between 4 h and 10 h in case of CSII (Figure 3, grey area). After this dip, a further upward trend of the luminescence decay times with increasing hydration time was observed. Especially, this dip is pointing to a strong and sudden (on the time scale of tenths of minutes to an hour) change of the Eu(III) coordination environment.

Apart from the shift of the dip, in principle a similar hydration time evolution of the luminescence behaviour of Eu(III) in both cement systems with water or tartaric acid was observed (Figure 3). In the case of citric acid, the addition of $CaSO_4$ (CSII) compared to $CaSO_4 \cdot 0.5H_2O$ (CSI) led to a longer τ_3 for the samples with hydration times < 4 h, but to shorter ones at longer hydration times. In the case of HCA addition, the trend was however the other way around. Here, the addition of $CaSO_4$ (CSII) led to shorter τ_3 in the first 4 h and longer ones at higher hydration times.

The short luminescence decay time τ_1 was nearly constant in all cases (CSI and CSII, Figure 3). In the case of CSI with water

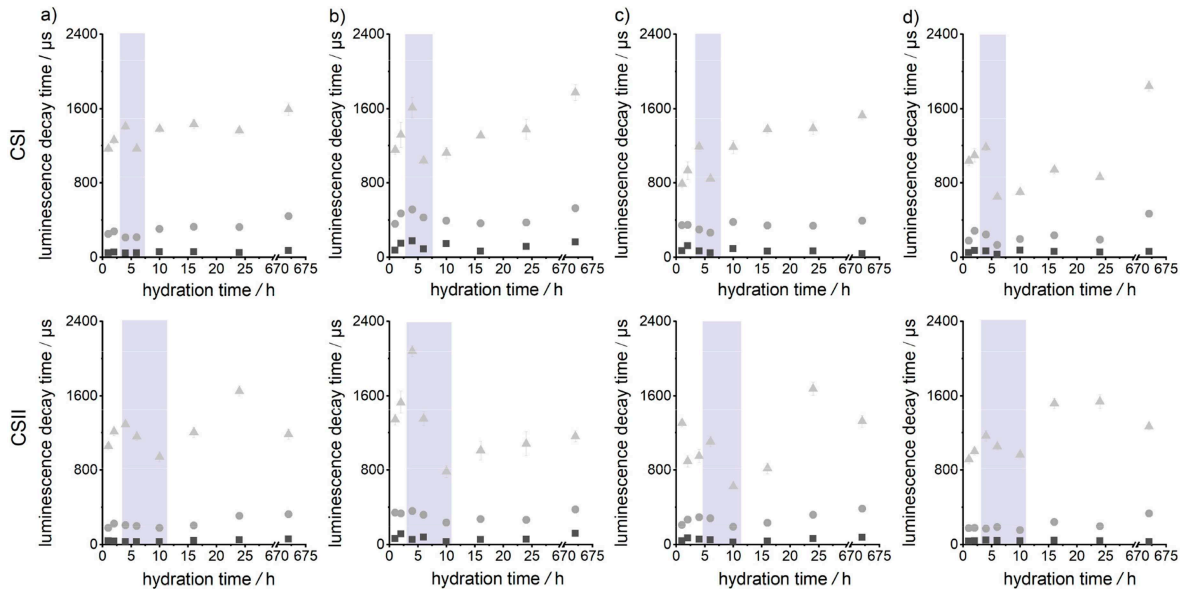

Figure 3. Hydration time *t* dependence of luminescence decay times τ_i for Eu(III) in CSI (top row) and CSII (bottom row) with a) water, b) citric acid, c) tartaric acid and d) HCA (▪ $\tau_{Eu(III)1}$ ($\Delta\tau_1 = \pm 50$ µs), ● $\tau_{Eu(III)2}$ ($\Delta\tau_2 = \pm 100$ µs), ▲ $\tau_{Eu(III)3}$ ($\Delta\tau_3 = \pm 150$ µs), $\lambda_{ex} = 394$ nm, emission of the $^5D_0 \rightarrow {}^7F_1$ as well as of the $^5D_0 \rightarrow {}^7F_2$ transition; grey area: dip of the luminescence decay times).

(Figure 3a, top row) and citric acid (Figure 3b, top row), similar luminescence decay times τ_3 were observed, whereas lower values in the first 6 h due to addition of tartaric acid were found (Figure 3c, top row). After 10 h hydration time, τ_3 of Eu(III) in CSI with tartaric acid reached similar values as with water or citric acid. However, the addition of HCA led to a decrease of τ_3 in the first 24 h of hydration (Figure 3d, top row). After 672 h, τ_3 was similar for CSI with water and tartaric acid as well as for citric acid and HCA. Furthermore, similar values were observed for the luminescence decay times τ_2 of Eu(III) in CSI after addition of water and tartaric acid. However, τ_2 of Eu(III) was shorter in the first 24 h after addition of HCA and longer in the first 6 h if citric acid was added. After 10 h hydration time, τ_2 of Eu(III) in the case of citric acid addition reached similar values as for water or tartaric acid addition. In the case of CSII, the addition of water and HCA led to similar luminescence decay times (τ_3 and τ_2) of Eu(III) in dependence to the hydration time (Figure 3a and 3d bottom row). In comparison, τ_3 was longer in the first 6 h and shorter between 10 h and 24 h in the case of citric acid addition (Figure 3b bottom row). After 672 h (28 d) an influence of citric acid was not observed. In the first 6 h τ_3 reached similar values by the addition of tartaric acid as of water, whereas they are shorter between 10 h and 16 h (Figure 3c bottom row). Afterwards, no difference of τ_3 was found. Compared to water, the addition of tartaric acid led to a slightly increased luminescence decay times τ_2 in the first 6 h, whereas no influence was observed afterwards. A similar behaviour was observed for citric acid addition. Here, τ_2 increased significantly in the first 10 h and is similar to values obtained for water afterwards.

2.4. TRLFS – Influence of Hydration Time on Luminescence Spectra and Relative Fractional Contributions

In all cases of CSI and CSII, the relative fraction of τ_1 decreased, while the one of τ_2 as well as τ_3 raised with increasing hydration time (Figure SI4). Furthermore, the highest fraction was observed for τ_1 and the lowest for τ_3.

Moreover, a change in the spectral signature of the Eu(III) emission spectrum (evaluated from TRANES) as well as a rise of the asymmetric ratio *R* with increasing hydration time was observed. Similar results were obtained for both analysed cement systems with all admixtures. At least two Eu(III) species can be distinguished due to the differences in the spectral intensity distribution only based on discrimination by increasing delay time used to record the emission spectrum. In Figure 4a–4c the TRANES of Eu(III) in CSI with HCA after different hydration times and the related change of the asymmetric ratio (Figure 4d) are shown as an example. Upon application of a more sophisticated data analysis method (PARAFAC, Figure SI5) the contribution of three different Eu(III) species are resolved complementary to the analysis of the luminescence decay kinetics (*vide supra*).

2.5. Connecting Spectroscopic Parameters with Location of Eu(III) in CSI and CSII

The observed spectroscopic parameters (decay kinetics, spectral intensity distribution, fractional intensities) are the result of Eu (III) to be located in different molecular environments. Different sorption sites of Eu(III) on or in the early hydration phases, e.g. portlandite, ettringite and C–S–H, are possible. Due to the similar coordination environments of Eu(III) on or in these phases, only small variations in the luminescence decay times are expected (Table SI4). However, to be able to specify the different Eu(III) species, the spectral information was analysed in more detail by dissembling the emission spectra with Gaussian curves (Eq. 8). Figure 5a shows the Gaussian fitting of the $^5D_0$-$^7F_2$ emission band of Eu(III) in CSI with HCA after 672 h (28 d) hydration time (at $t_l = 1000$ µs). The measured $^5D_0$-$^7F_2$ emission bands of Eu(III) in the reference systems, e.g. Eu(III) in portlandite (yellow), ettringite (green), C–S–H (pink), and Eu(III)-carbonate (blue), are shown in the Figure 5b. The sum of the reference spectra (represented by Gaussian curves) of Eu(III) (red) is in good agreement with the measured emission band (black) (Figure 5a). Further examples for the Gaussian fitting of Eu(III) in CSI and CSII showing an excellent agreement are presented in the SI (Figure SI6 and SI7).

The relative fractions of the single Eu(III) components (Eu(III) in portlandite, ettringite and C–S–H) in CSI and CSII were calculated using Eq. 10 and are shown in Figure 6. These fractions show on which hydration phase the Eu(III) preferentially interacts. In the time-resolved luminescence experiments the initial gate step was applied as a selection criterion, e.g.

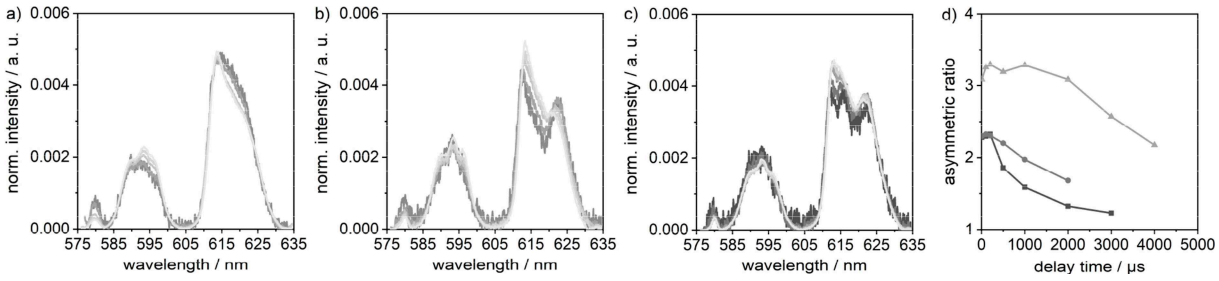

Figure 4. TRANES of Eu(III) in ZSI with HCA after a) 1 h, b) 24 h and c) 672 h hydration time ($\delta t = -10$ µs, -100 µs, -200 µs, -500 µs, -1000 µs, -2000 µs and -3000 µs, complies from bright grey to dark grey; $\lambda_{ex} = 394$ nm) as well as d) the related asymmetric ratios *R* in dependence on the delay time t_l (-- 1 h, -•- 24 h and -▲- 672 h).

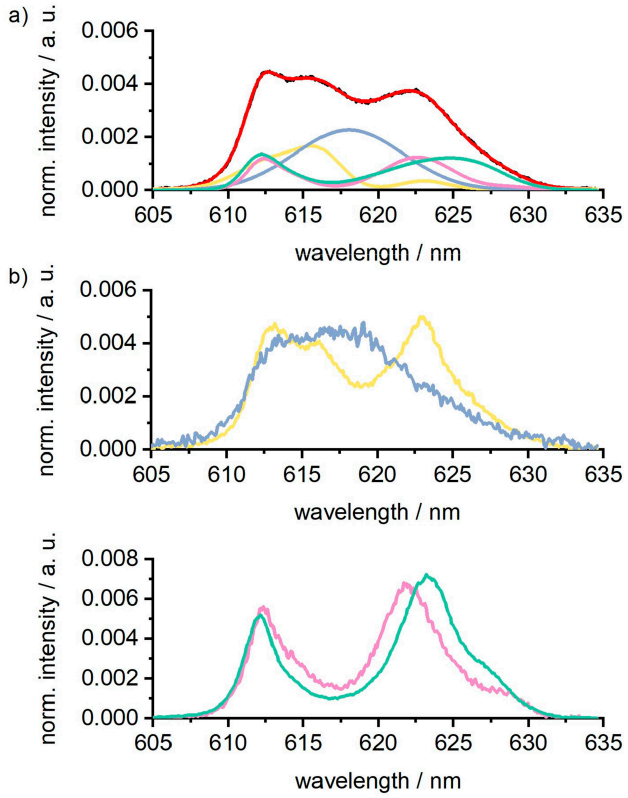

Figure 5. a) Gaussian fitting (red) of the measured $^5D_0$-$^7F_2$ emission band of Eu(III) (–) in CSI with HCA after 28 d hydration time (delay time $t_i = 1000$ µs, $\lambda_{ex} = 394$ nm) and b) $^5D_0$-$^7F_2$ emission band of the references (yellow: Eu(III) in portlandite ($t_i = 200$ µs), blue: Eu(III)-carbonate (p$H = 12.0$, $t_i = 1013$ µs), margenta: Eu(III) in C–S–H (C/S = 1.4, p$H = 12.6$, $t_i = 1730$ µs), and green: Eu (III) in ettringite (p$H = 12.6$, $t_i = 1730$ µs)).

sorbed species were detected in favour over hydroxide species (the latter do have a relatively short luminescence time and hardly contribute to the luminescence signal detected at large initial delays). Consequently, the fractions shown are only relative and directly correlated to the gating settings.

High fractions of Eu(III) in portlandite were observed for CSI for the whole analysed hydration time period (Figure 6a, top). For Eu(III) in CSII with citric acid or tartaric acid similar results were found (Figure 6b, top). In contrast, for CSII with water or HCA an Eu(III) sorption on portlandite was observed earliest after 24 h.

In the case of CSI with citric acid as well as HCA Eu(III) sorbs to C–S–H (Figure 6a, middle) starting after 1 h hydration time and was observed over the whole analysed hydration time period as well. However, in the case of CSI with tartaric acid an Eu(III) sorption to C–S–H was found earliest after 4 h and with water addition even later after 10 h. In the case of CSII an Eu(III) sorption to C–S–H was observed with tartaric acid addition after 24 h, with citric acid after 10 h. In contrast with water as well as with HCA Eu(III) on C–S–H was detected after only 1 h hydration time (Figure 6b, middle).

Eu(III) sorbed to ettringite was found in both cement systems with water in the whole hydration time period, whereas this sorption was retarded for all admixtures (Figure 6a and 6b, bottom). For CSI with tartaric acid or HCA Eu(III) sorbed to ettringite was observed earliest after 4 h and with citric acid after 16 h (Figure 6a below). The addition of HCA to CSII led to a sorption of Eu(III) to ettringite after 6 h (Figure 6b below). A fraction of Eu(III) sorbed to ettringite was observed after 10 h for CSII with citric acid and after 672 h (28 d) with tartaric acid.

In general, the fractions of Eu(III) sorbed to C–S–H or ettringite are in both cement systems (CSI and CSII) lower compared to Eu(III) in portlandite (Figure 6).

The formation of Eu(III)-carbonate and the sorption of Eu(III) to $CaSO_4$ (only in CSII) are side reactions and do not play a role in the assessment of the additive influence on the hydration process. For reasons of completeness, the fractions of both in the cement samples are illustrated in Figure SI8 and the $^5D_0$-$^7F_2$ emission band of Eu(III) in $CaSO_4$ in Figure SI9.

3. Discussion

The aim of the work was to analyse the influences of different admixtures on the hydration of cement paste. For this, cement paste samples after different ageing duration were analysed by XRD, SEM, and TRLFS to obtain detailed and complementary information on the phase composition. The latter included the unhydrated cement phases, as well as their hydrates formed during the hydration process over hours up to 28 days. The phases of the unhydrated cement are crystalline and accessible for conventional XRD. The hydrate phases include different crystalline phases also accessible by the XRD, and poorly crystalline C–S–H mostly hidden for this analytical method. The XRD analysis allows to determine the percentages of the crystalline phases after fixed ageing times and based on these data to compare the role of admixtures on the corresponding hydration reactions. Thus, strong influences of the admixtures on the aluminate reactions were identified by analysing the increase of ettringite percentages and corresponding decrease of the aluminate percentages in different cement paste samples. Controversial dependence of the ettringite percentage from the kind of admixture was found for both analysed cement systems.

In CSI (containing $CaSO_4 \cdot 0.5H_2O$), the presence of admixtures led to an intensive aluminate hydration as the higher amount of ettringite was found to be formed in contrast to the reference sample. In CSII, the formation of ettringite was decreased in presence of admixtures. From all three admixtures used, the citric acid was the one most distinctly changing the amount of ettringite in contrast to the reference sample for both analysed cement systems. In CSI, it led to the formation of the highest amount of ettringite, and in CSII – of the lowest. For the assessment of the silicate reaction, the changes in the amounts of its products portlandite and C–S–H are needed to be considered. Similar to the aluminate reaction, the silicate reaction was intensified in CSI and decelerated in CSII as estimated on the amount of portlandite. Here, the tartaric acid had the strongest influence on the amount of portlandite formed, leading to the formation of highest amount of portlandite in CSI and lowest in CSII in comparison to all other

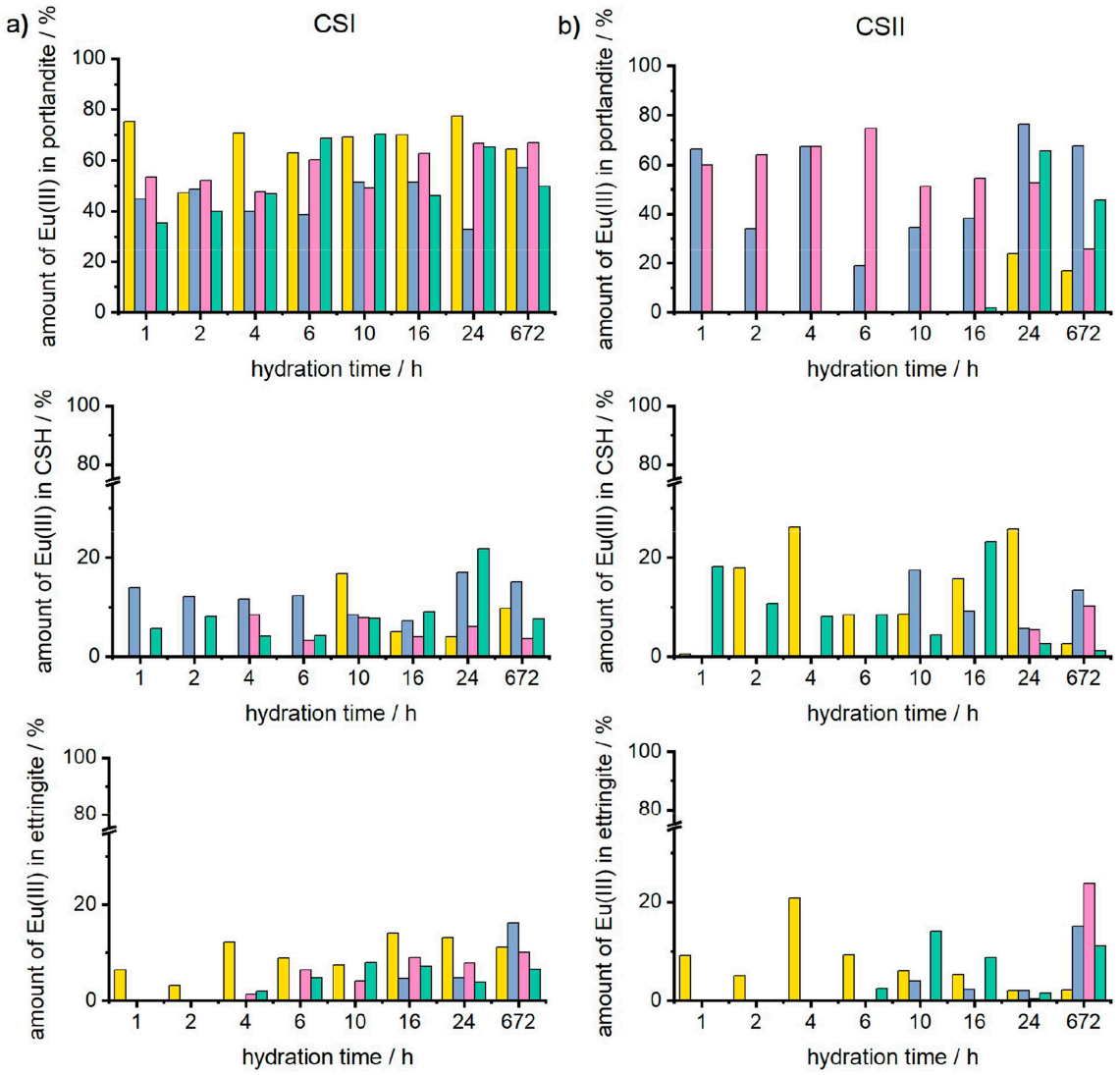

Figure 6. Amount of Eu(III) in portlandite (top), C–S–H (middle) and ettringite (bottom) in a) CSI as well as b) CSII in dependence on the hydration time (admixtures: yellow - water, blue - citric acid, magenta - tartaric acid and green - HCA (delay time $t_l = 1000$ µs, $\lambda_{ex} = 394$ nm, $\Delta f = \pm 20\%$).

samples. The strongest increase of the portlandite percentage in CSI was found in the cement paste with tartaric acid and lowest in the reference sample. Controversially for CSII, the highest percentage of portlandite was found in the reference cement paste and the lowest in the cement paste with citric acid. In summary, according to the XRD data, the presence of admixtures has similar influence on the crystalline components of the analysed cement systems: the aluminate and silicate reactions are accelerated in CSI and decelerated in CSII, whereas citric or tartaric acids were the admixtures with the most significant effects in CSI or CSII, respectively. Moreover, the presence of admixtures seems to change the kinetics of the hydration reaction and consequently the amounts of related hydrates formed.

SEM imaging revealed the morphology of the crystals formed on the surfaces of the non-hydrated cement particles. It was seen that the surface coverage of the initial cement particles with hydration products was growing with increasing hydration time. Morphological changes of ettringite crystals were observed depending on the cement system (CSI vs. CSII) and on the presence of admixtures. In CSI, the ettringite crystals were well-shaped hexagonal prisms, whereas in CSII they appeared thin and forming a straw-like cover on the cement particles. In presence of admixtures, the visibly lower number of larger ettringite crystals was formed. Obviously, a lower number of seeds can be formed, if an admixture is added to the cement system. This makes it attractive to assume, that admixtures seem to distort the ettringite nucleation. In our previous work, we could show the occupation of the ettringite nucleation places by the admixtures carrying the negative charges (like negatively charged carboxylic groups available in each admixture analysed in this study).[9] The nucleation of ettringite is possibly shifted from the cement particle surface into the surrounding solution, thus explaining the rise of the ettringite amount in presence of such admixtures as discussed above. Additionally, a lower number of larger crystals could be visually

identified on the SEM images. Obviously, the aluminate reaction is balanced between nucleation on the cement surface and in the surrounding solution. Consequently, the amount of ettringite formed changes depending on how favourable the conditions are for its crystallization. According to SEM imaging, the formation of C–S–H was more pronounced in the cement samples based on CSI. The presence of any admixture in each cement system led to the formation of the C–S–H cover, that was visually less dense in comparison to the corresponding admixture-free reference sample.

Eu(III) serve as a luminescence sensor due to its specific luminescence response on the coordination environment. Especially, poorly crystalline hydrate phases (such as C–S–H) with a high Eu(III) sorption affinity become accessible. In a control experiment ICP-MS analysis of Eu(III) sorbed on C–S–H (C/S = 1.4, pH = 12.6, 10 µmol Eu(III)/g C–S–H) showed an exchange of every 1670 Ca(II) ion against one Eu(III) ion. This underlines that only an influence of the Eu(III)-sorption to the hydration process of the CSs is not expected. Therefore, additional information on the formation of hydrate phases can be obtained complementary to XRD and SEM data.

By repeating the TRLFS measurements at different sites of the grounded cement sample and after a certain time similar data were observed and leads to representative results. Three different Eu(III) species were identified based on the temporal and spectral analysis of the luminescence data. The formation of Eu(III)-hydroxide is indicated by the calculated short decay times τ_1 (Figure 3), the spectral signature of the $^5D_0$-$^7F_2$ emission band (at a delay time of $t_l = 10$ µs) (Figure 4) and was observed in absence of influences of admixture, type of the sulphate carrier ($CaSO_4$ or $CaSO_4 \cdot 0.5H_2O$) or hydration time. This is in good agreement with the observations by Burek *et al.*.[10] The luminescence of the other two Eu(III) species is characterized by their long luminescence decay times (τ_2 and τ_3) indicating a significantly decreased quenching rate due to a reduced number of OH-oscillators in the coordination sphere. Therefore, this is pointing to surface sorption on or incorporation of Eu(III) into the hydrate phases that are formed over time. A similar sorption process of Eu(III) on C–S–H was observed before.[19–22] A shorter luminescence decay time τ_3 of Eu(III) was observed in CSI with tartaric acid (in the first six hours) and with HCA (in the first 24 hours) compared to CSI reference or with citric acid. This effect points to more OH-vibrations in the first coordination sphere of Eu(III) and, consequently, to less incorporation of Eu (III) into the hydrate phases, thus indicating a variation of the hydrate phase composition (Figure 3).

Studies of the cement hydration process describe a beginning C–S–H formation between 1 h and 6 h.[23–25] This corresponds to the time range of the observed dip of hydration-related time dependence of the luminescence decay times that was found for the early hydration times (s. Figure 3). As discussed above, this dip indicates a strong short-term change of the Eu(III) coordination environment and could result from a changed hydrate phase composition. Except for CSI with water and CSII with citric acid, the factor analysis (Figure 6a and 6b, middle) suggests the existence of C–S–H in the hydration time range between 1 h and 6 h for all the other analysed systems. In good agreement with the dip is only the beginning Eu(III) sorption on C–S–H in the case of CSI with tartaric acid. The SEM analysis, however, shows a visible C–S–H formation in CSI not before 4 h hydration time. It is described in the literature, that C–S–H phases differ in their structure and density at early hydration stages. At the hydration begin, an intermediate C–S–H phase is observed, which differs structurally from the more mature C–S–H. Thus, the observed dip in the hydration-related time dependence of the luminescence decay times and its controversy to SEM observations can be related to the transformation of the intermediate C–S–H to the mature product, thus explaining the abrupt change in the nearest coordination environment of Eu(III).[26–28]

The change of the luminescence decay times with prolonged ageing indicates a progressive sorption of Eu(III) on the surface of as well as an incorporation into the hydrate phases and a decrease in the amount of Eu(III)-hydroxide (Figure SI4). Furthermore, the amount of Eu(III) surface complexation is higher than that of Eu(III) incorporation. The change of the spectral signature of the Eu(III) emission in the TRANES with increasing hydration times indicates a change of the Eu(III) species. Moreover, it is a consequence of a progressive sorption and of a change of the hydrate phase composition (Figure 4).

Similar sorption sites can be further distinguished by the detailed analysis of the information hidden in luminescence spectra by fitting of Gaussian curves. This analysis shows for both cement systems only a small amount of Eu(III) localized in C–S–H or ettringite, but a higher one in portlandite (Figure 6). This indicates a strong sorption affinity of Eu(III) to portlandite considering the fact of a higher amount of ettringite in the system according to the XRD data (Figure 1). Moreover, the addition of admixtures to both cement systems retards the ettringite formation (Figure 6). In the case of CSI, tartaric acid and HCA have similar effects, and citric acid – the strongest one, whereas in the case of CSII tartaric acid has the strongest influence. In contrast, for CSI a similar retarded effect of both acids and the strongest by the addition of HCA was observed by XRD. In good agreement are the SEM results, which indicate a faster formation of ettringite for CSI and CSII with water (reference system) compared to the samples with admixture presence due to the formation of numerous smaller crystals. A retarded ettringite formation by the addition of citric and tartaric acid was already observed before.[3,7] Furthermore, the TRLFS data show an increasing amount of ettringite with increasing hydration time for CSI and are in good agreement with the observation by XRD. However, SEM and XRD are pointing to an early formation of ettringite after 1 h hydration time for both cement systems, whereas this was not observed in all cases by TRLFS. This could be caused by a preferred sorption of Eu(III) to portlandite (*vide supra*) and to $CaSO_4$ (in CSII), as well as by the formation of Eu(III)-carbonate, which all compete with the sorption to ettringite. Therefore, a strong incorporation of Eu(III) into ettringite and the specific influence on the spectral signature is weak after 1 h hydration time.

The TRLFS data showed an accelerated C–S–H formation in CSI due to the addition of admixtures. Here, citric acid and HCA had the strongest influence. For CSII, the addition of citric or

tartaric acid, however, led to a retarded C–S–H formation, whereas citric acid had the most pronounced effect. Furthermore, a retarded C–S–H formation in CSII explains the later dip of the luminescence decay times τ_2 and τ_3 as compared to the one observed for CSI (Figure 3).

TRLFS indicates portlandite formation in both cement systems already after shorter hydration times if compared to XRD. The reason could be the high sorption affinity of Eu(III) to this hydration phase. For CSI, the sorption of Eu(III) to portlandite was observed for the whole hydration time range investigated and no influence of the admixtures was found. In CSII, water (reference system) and HCA retarded the portlandite formation significantly.

It is tempting to attribute the contradictory influence of admixtures on the C–S–H as well as portlandite formation in CSI and CSII to the different types of sulphate carrier used in the preparation. The anhydrous $CaSO_4$ in CSII has a lower solubility than $CaSO_4 \cdot 0.5H_2O$ in CSI. Consequently, less Ca(II) (important for C–S–H and portlandite formation) and SO_4-ions (for ettringite formation) are freely available in CSI. The discussed above distinct differences in the morphology of the ettringite crystals in both cement systems confirm this effect.

The complementary use of XRD, SEM and TRLFS allowed deep insights into the admixture action in cementitious systems differing by the kind of the sulphate carrier (CSI with $CaSO_4 \cdot 0.5H_2O$; CSII with $CaSO_4$). The changes in the amounts of the specific crystalline reaction products are available from the XRD data. According to them, the most significant intensification of the aluminate reaction was observed in CSI, if citric acid was added. The silicate reaction was the most intensive after the addition of tartaric acid. Reverse effects were observed with these admixtures in CSII. The addition of citric acid slowed down the aluminate reaction in CSII; the addition of tartaric acid most significantly delayed the silicate reaction. However, it should be noted, that the extent of the silicate reaction could be estimated on the amount of portlandite. Another important product of this reaction, which is the main binding phase in hardened cement systems, the C–S–H phase, was inaccessible via XRD due to its poor crystallinity. The use of SEM allowed visual assessments of the admixture effects based on the appearance of the hydration products. Significant differences were revisited between CSI and CSII reference samples, as well as those with particular admixture if correspondingly compared. The use of SEM allowed first insights into the formation of C–S–H, since this phase formed a characteristic cover on the unhydrated cement particles. Further information on C–S–H was however still inaccessible. The application of TRLFS allowed detailed insights into the phase composition of the sample based on the specific sensitivity of Eu(III) used as a sensor to its chemical surrounding. The identification of the phases contributed to the luminescence reply of cement systems was achieved by comparison with the spectra of corresponding pure compounds and following deep mathematical analysis of the spectral data of the analysed samples by considering the conclusions from the XRD data. The extent of the Eu(III) sorption affinity to particular phases was needed to be considered during the data analysis. TRLFS results confirmed the conclusions from the XRD data about the reverse effects of admixtures on silicate and aluminate reactions in both analysed cement systems. Additionally, the formation of portlandite, which indicates the ongoing silicate reaction, was identified earlier than by XRD due to high sensitivity of the Eu(III) used as luminescence sensor. Furthermore, the luminescence data allowed to identify the formation of C–S–H, as well as the change in its structure between 4 h and 6 h of ageing. Thus, the detailed comparison of the information obtained from XRD, SEM and TRLFS enabled comprehensive insights into the phase formation during the hydration taking place in the complex cementitious systems influenced by chemical admixtures.

4. Conclusions

We have presented complementary data of different analytical methods (XRD, SEM, TRLFS) to describe the effect of organic admixtures on the hydration process of two cement systems. Different observation scales of the methods applied allow to reach an extensive complementary information about the changes in the cement paste composition due to the influences of the chemical admixtures. XRD allows to monitor the crystalline amounts of the cement paste components and SEM – to analyse the formation of hydrate phases based on their morphology. The results show, if admixtures were used, a changed hydration reaction kinetics, whereas the hydration products remain the same and differ exclusively in their amounts considering the specific ageing time. With the use of Eu(III) as an optical probe in TRLFS analysis, it was possible to add additional information on the hydration phase dynamics due to the complementary selectivity of the Eu(III) sorption affinity to the hydration phases. Furthermore, the TRLFS also allowed to monitor minor phase (portlandite), which has a high sorption affinity for Eu(III). It was for the first time possible to get insights into the influences of admixtures on the C–S–H formation using luminescence spectroscopy. The dip in the luminescence decay times indicates possibly the transition of the low-density C–S–H formed at the hydration begin into high-density C–S–H characteristic for mature cement paste. Further work is needed to directly evidence this dip to specific structural changes of C–S–H during the hydration process.

In the future, the combination of SEM, XRD and TRLFS might become a key tool for the cement industry. Especially, online and inline luminescence measurements in combination with fiber optics may pave the road to novel cement materials based on an improved understanding of the cement hydration and how this process can be directed. Here, the outstanding sensitivity and the non-invasive character of optical methods will help to further decipher molecular processes during the hydration of cement. Luminescence spectra can be measured in a few seconds and it is foreseen to also test additional luminescence probes (such as other lanthanide, but also organic dyes maybe of interest) in order to establish a mulitparameter sensing for a further improved understanding of cement hydration kinetics. Here, it can be expected that the achievable time-resolution is determined by mixing times of the

cement components, which probably is on the time-scale of minutes.

Acknowledgements

Katja Burek is thankful to the Federal Ministry of Economic Affairs and Energy (reference no 02E11415F) for the financial support. Julia Stroh thanks Torvid Feiler for the support in the sample preparation. The authors acknowledge the support of the Deutsche Forschungsgemeinschaft and Open Access Publishing Fund of University of Potsdam.

Conflict of Interest

The authors declare no conflict of interest.

Keywords: cement admixtures · cement hydration · Europium · luminescence · SEM · X-ray diffraction

[1] D. E. Macphee, E. E. Lachowski in *Cement Components and Their Phase Relations, Vol. 3*, Butterworth-Heinemann, Oxford, **1998**, 95–129.
[2] J. Cheung, A. Jeknavorian, L. Roberts, D. Silva, *Cem. Concr. Res.* **2011**, *41*, 1289–1309.
[3] G. Möschner, B. Lothenbach, R. Figi, R. Kretzschmar, *Cem. Concr. Res.* **2009**, *39*, 275–282.
[4] X. W. Zhang, C. X. Lu, J. Y. Shen, *Constr. Build. Mater.* **2016**, *112*, 877–884.
[5] G. Kastiukas, X. Zhou, J. Castro-Gomes, S. Huang, M. Saafi, *Constr. Build. Mater.* **2015**, *101*, 389–395.
[6] G. Velazco, J. M. Almanza, D. A. Cortes, J. C. Escobedo, J. I. Escalante-Garcia, *Mater. Constr.* **2014**, *64*, e036.
[7] M. Bishop, A. R. Barron, *Ind. Eng. Chem. Res.* **2006**, *45*, 7042–7049.
[8] M. C. Schlegel, A. Sarfraz, U. Müller, U. Panne, F. Emmerling, *Angew. Chem. Int. Ed.* **2012**, *51*, 4993–4996; *Angew. Chem.* **2012**, *124*, 5078–5081.
[9] J. Stroh, M. C. Schlegel, W. Schmidt, Y. N. Thi, B. Meng, F. Emmerling, *Constr. Build. Mater.* **2016**, *106*, 18–26.
[10] K. Burek, F. Krause, M. Schwotzer, A. Nefedov, J. Sussmuth, T. Haubitz, M. U. Kumke, P. Thissen, *ACS Sustainable Chem. Eng.* **2018**, *6*, 14669–14678.
[11] J. Dengler, C. Hesse, S. Seufert in Hydration control mixture for mortar and cement compositions, Vol. WO 2017/212044A1, DPMAregister, **2017**, 56.
[12] R. Snellings, J. Chwast, Ö. Cizer, N. De Belie, Y. Dhandapani, P. Durdzinski, J. Elsen, J. Haufe, D. Hooton, C. Patapy, M. Santhanam, K. Scrivener, D. Snoeck, L. Steger, S. Tongbo, A. Vollpracht, F. Winnefeld, B. Lothenbach, *Mater. Struct.* **2018**, *51*, 111.
[13] W. Franus, R. Panek, M. Wdowin, *2nd International Multidisciplinary Microscopy and Microanalysis Congress.* **2015**, 164, 105–112.
[14] P. C. Fonseca, H. M. Jennings, *Cem. Concr. Res.* **2010**, *40*, 1673–1680.
[15] Z. D. Zhang, G. W. Scherer, A. Bauer, *Cem. Concr. Res.* **2018**, *107*, 85–100.
[16] K. Scrivener, R. Snellings, B. Lothenbach, *A Practical Guide to Microstructural Analysis of Cementitious Materials*, CRC Press **2015**, 21–28.
[17] R. Bro, *Chemom. Intell. Lab. Syst.* **1997**, *38*, 149–171.
[18] B. Drobot, R. Steudtner, J. Raff, G. Geipel, V. Brendler, S. Tsushima, *Chem. Sci.* **2015**, *6*, 964–972.
[19] P. Mandaliev, T. Stumpf, J. Tits, R. Dahn, C. Walther, E. Wieland, *Geochim. Cosmochim. Acta.* **2011**, *75*, 2017–2029.
[20] I. Pointeau, B. Piriou, M. Fedoroff, M. G. Barthes, N. Marmier, F. Fromage, *J. Colloid Interface Sci.* **2001**, *236*, 252–259.
[21] M. L. Schlegel, I. Pointeau, N. Coreau, P. Reiller, *Environ. Sci. Technol.* **2004**, *38*, 4423–4431.
[22] J. Tits, T. Stumpf, T. Rabung, E. Wieland, T. Fanghanel, *Environ. Sci. Technol.* **2003**, *37*, 3568–3573.
[23] *Zement Taschenbuch*, Verein Deutscher Zementwerke e. V. (Hrsg.) by Verlag Bau + Technik GmbH, Düsseldorf, **2002**, 109–124.
[24] I. Odler in *Hydration, Setting and Hardening of Portland Cement, Vol. 6* (Ed. P. C. Hewlett), Butterworth-Heinemann, Oxford, **1998**, 241–297.
[25] F. W. Locher, W. Richartz, S. Sprung, *ZGK.* **1976**, *29*, 435–442.
[26] E. Gallucci, P. Mathur, K. Scrivener, *Cem. Concr. Res.* **2010**, *40*, 4–13.
[27] J. W. Bullard, H. M. Jennings, R. A. Livingston, A. Nonat, G. W. Scherer, J. S. Schweitzer, K. L. Scrivener, J. J. Thomas, *Cem. Concr. Res.* **2011**, *41*, 1208–1223.
[28] X. D. Cong, R. J. Kirkpatrick, *Cem. Concr. Res.* **1993**, *23*, 1065–1077.

Manuscript received: July 25, 2019
Revised manuscript received: November 9, 2019